

## Supplemental Material

**Energy function for soft, deformable particles:** The energy function in Eq. 1 below can be used to model a wide range of soft and deformable particles.

$$U = \frac{k_l N_v}{2} \sum_{m=1}^N \sum_{i=1}^{N_v} (l_{m,i} - l_0)^2 + \gamma \sum_{m=1}^N \sum_{i=1}^{N_v} l_{m,i} + \frac{k_a}{2} \sum_{m=1}^N (a_m - a_0)^2 + \frac{k_b}{2N_v} \sum_{m=1}^N \sum_{i=1}^{N_v} \left( \frac{2(\hat{l}_{m,i} - \hat{l}_{m,i+1})}{l_{m,i} + l_{m,i+1}} \right)^2, \quad (1)$$

where  $k_l$  is the contractility per vertex,  $\gamma$  is the line tension,  $k_a$  is the elastic constant for area fluctuations,  $k_b$  is the bending rigidity per vertex, and  $N$  is the number of deformable polygons with  $N_v$  vertices. The bond vector  $\vec{l}_{m,i} = \vec{v}_{m,i+1} - \vec{v}_{m,i} = l_{m,i} \hat{l}_{m,i}$ ,  $\vec{v}_{m,i}$  is the position of the  $i^{\text{th}}$  vertex on polygon  $m$ , and the prime on the sum in the last term of Eq. 1 indicates that it is cyclic, so that the bond vector  $\vec{l}_{m,N_v}$  connects vertex  $i=N_v$  and  $i=1$ . Note that the expression for  $U$  in Eq. 1 is independent of  $N_v$  in the large- $N_v$  limit. By tuning the parameters in Eq. 1, it can be used to model a variety of soft particulate systems, such as cell monolayers, bubbles/emulsions, solid shells, soft solid particles, and vesicles as shown in Table S.1. To model vesicles, which do not possess an in-plane shear modulus, the first term in Eq. 1 is changed to be a purely repulsive linear spring potential.

Table S.1 Five prototypical soft, particulate systems and the parameters  $k_l$ ,  $\gamma$ ,  $k_a$ , and  $k_b$  in Eq. 1 that would be used to model them.

System	$k_l$	$\gamma$	$k_a$	$k_b$
Cell monolayers	$>0$	$=0$	$>0$	$\geq 0$
Bubbles/emulsions	$=0$	$>0$	$>0$	$=0$
Solid shells	$>0$	$=0$	$=0$	$>0$
Soft solid particles	$>0$	$=0$	$>0$	$>0$
Vesicles	$=0$ for $l_{m,i} > l_0$ $>0$ for $l_{m,i} < l_0$	$>0$	$>0$	$>0$

**Simulation method:** We study DP packings containing from  $N=64$  to  $N=1000$  deformable polygons. To generate DP packings, we place polygons with random locations and orientations in a square box with periodic boundary conditions at initial packing fraction  $\phi=0.2$ . We successively compress (or decompress) the system boundaries isotropically using small increments  $\Delta\phi=10^{-4}$  and minimize the total potential energy (Equations 2 and 3 in the manuscript) per particle  $U/N$  after each compression (or decompression step) using over-damped molecular dynamics simulations until the kinetic energy per particle satisfies  $K/N < 10^{-20}$ . The system is decompressed when  $U/N$  at a local minimum is nonzero, i.e. there are finite particle overlaps. If  $U/N$  is “zero” (i.e.  $U/N < 10^{-16}$ ), the system is compressed. The increment by which  $\phi$  is changed at each compression or decompression step is gradually decreased. This method yields mechanically stable packings at jamming onset, satisfying  $0 < U/N < 10^{-16}$  and  $K/N < 10^{-20}$ .

**Potential energy at confluence:** Figure S1 shows that the total potential energy  $U/N$  at confluence,  $\phi = \phi_{max}$ , depends on the shape parameter  $A$ . We apply quasistatic isotropic compression in steps of  $\Delta\phi=10^{-4}$

followed by energy minimization to compress DP packings at jamming onset  $\phi_j(A)$  to  $\phi_{max} \approx 0.95$  for the rough surface method with  $N_v=12$ . In Fig. S1 (a), we show  $U/N$  versus packing fraction  $\phi$  over a range of  $A$  from 1.02 to 1.25. In Fig. S1 (b), we plot  $U(\phi_{max})/N$  versus  $A$ , which shows a sharp decrease as  $A$  increases above  $A^* \approx 1.16$ . Similar results have been found in Ref. [11] in the main text, where the authors used the vertex model to show that confluent cell monolayers undergo a rigidity transition from solid-like states for  $A < A^*$  to liquid-like states for  $A > A^*$ . In this Letter, we help explain the rigidity transition discussed in Ref. [11]. Packings of deformable particles with asphericity  $A < A^*$  are compressed at confluence since  $\phi_j(A) < \phi_{max}$ . In contrast, confluent systems are close to jamming onset for all  $A > A^*$ .

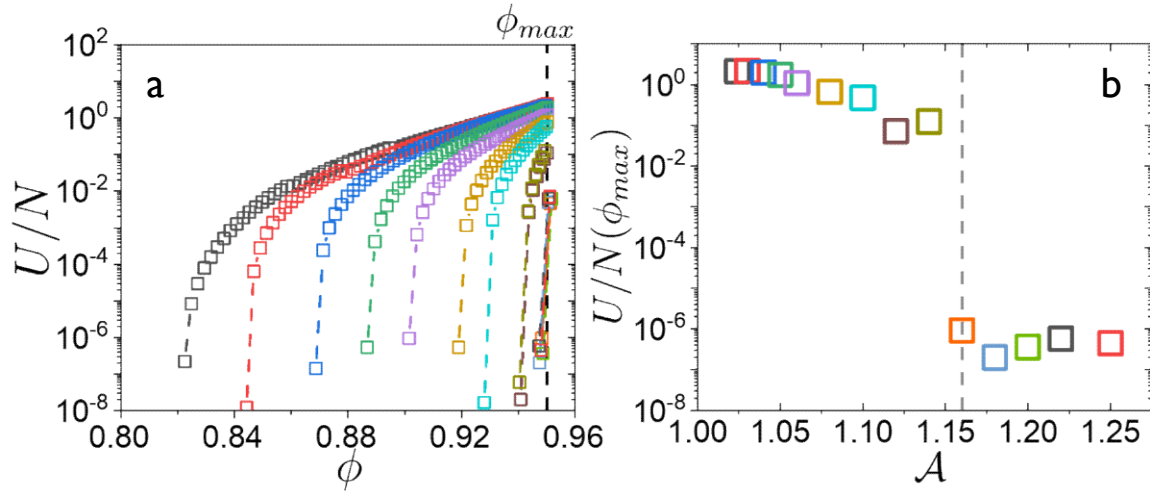


Figure S1: (a) Total potential energy per particle  $U/N$  as a function of packing fraction  $\phi$  for DP packings with  $N=64$  using the rough surface method with  $N_v=12$ . The asphericity  $A$  increases from left to right from  $A=1.02$  to  $1.25$ . The dashed vertical line indicates the maximum packing fraction  $\phi_{max}$  for this rough surface method. (b)  $U/N$  at confluence versus the asphericity  $A$ . The vertical dashed line indicates  $A=A^*$ .

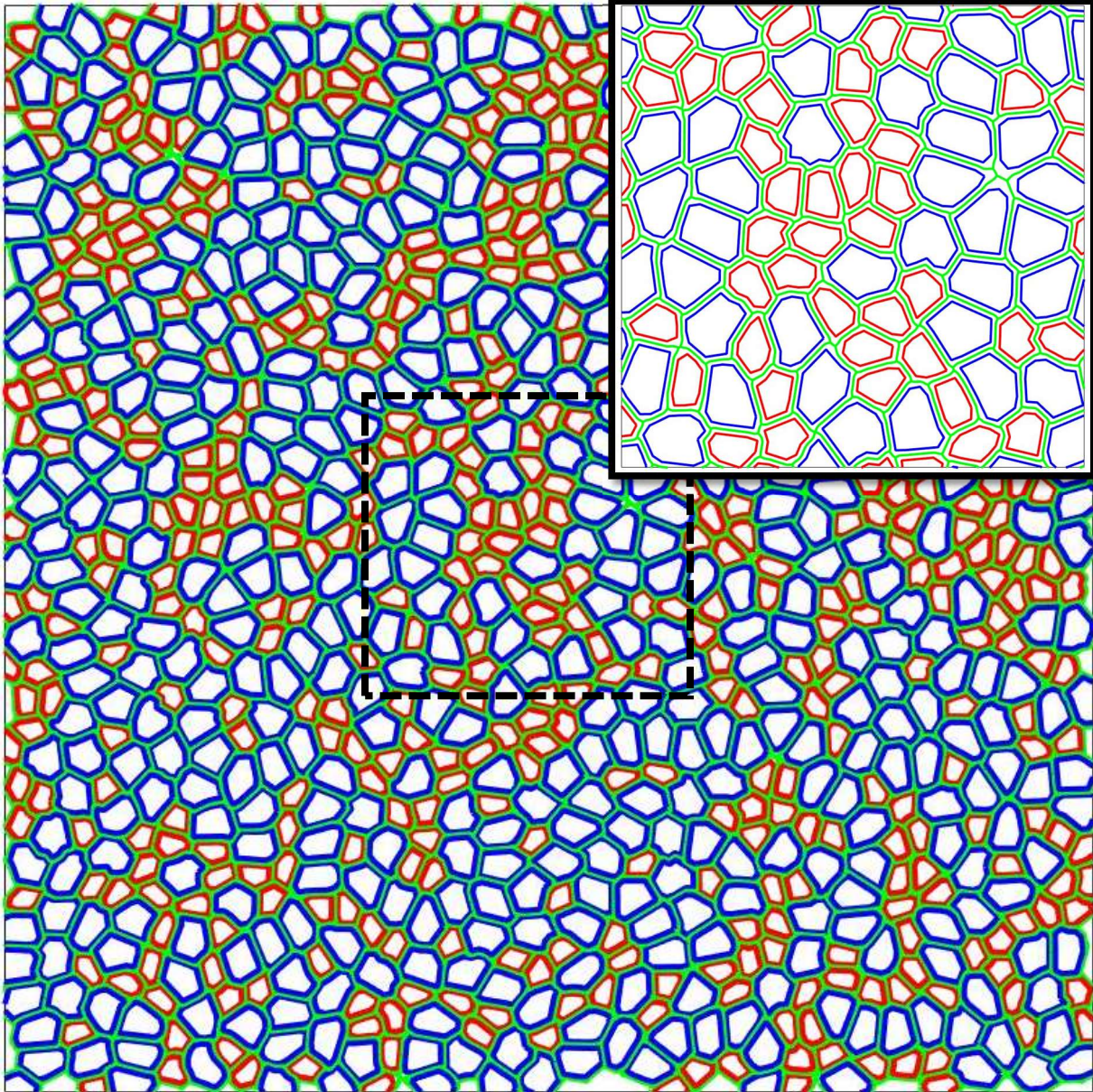


Figure S2: Packing of  $N=1000$  bidisperse deformable polygons with asphericity  $A=1.22$  (half large and half small with perimeter ratio  $r=1.4$ ). The number of vertices for the small particles (red) is  $N_v=12$ , while the large particles (blue) have  $N_v=17$ . The surface-Voronoi cell for each particle is shown in green. The inset shows an enlarged view of the area within the region indicated by the dashed black line.

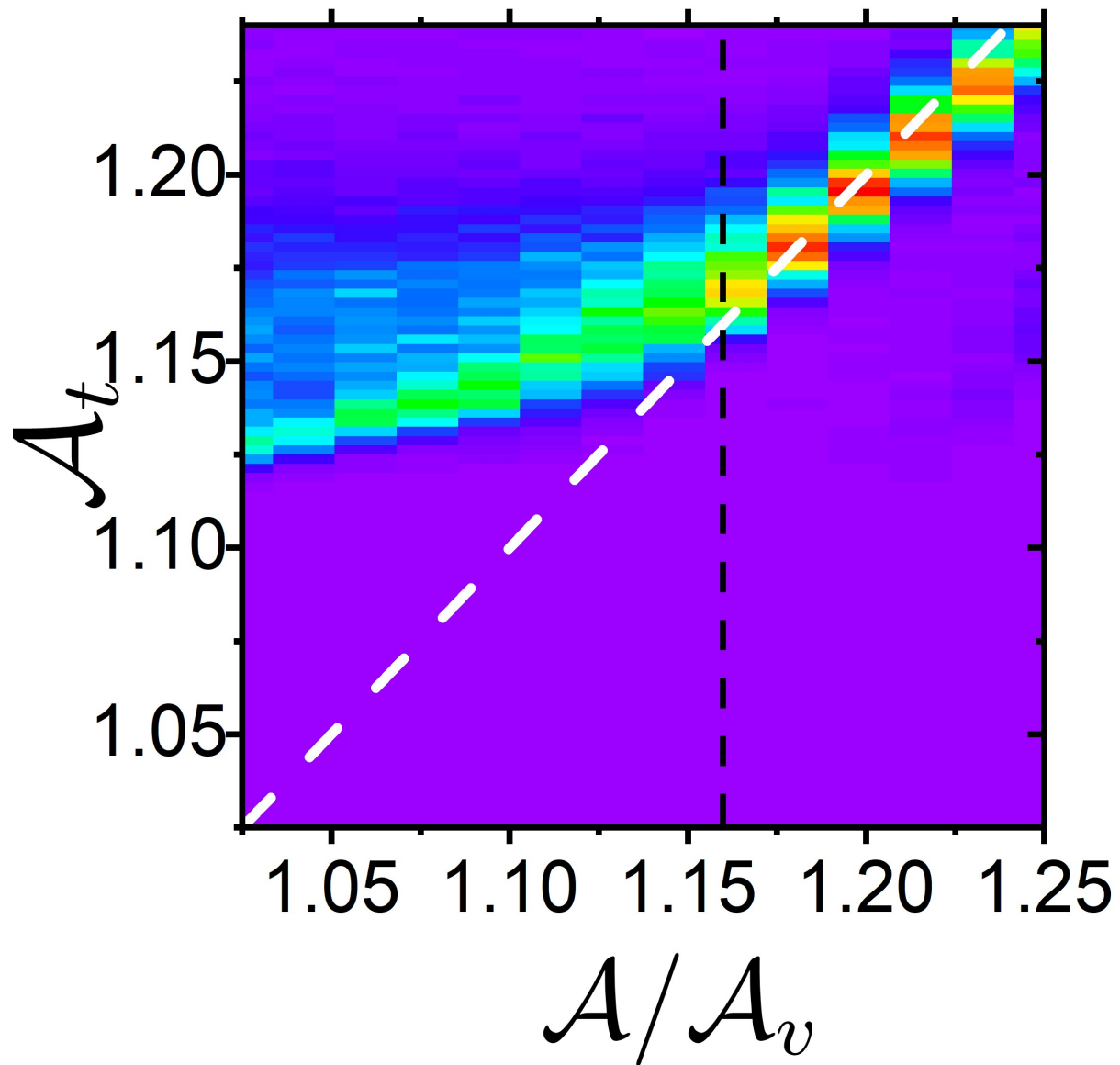


Figure S3: Color map showing the histogram of the asphericity of the surface-Voronoi cells  $A_t$  versus the asphericity  $A/A_v$  of packings of monodisperse deformable particles with  $N=64$ , using the rough surface method with  $N_v=12$ . The probability for a given  $A_t$  increases as the color varies from blue to red. The dashed vertical black line indicates  $A^*=1.16$ . For  $A < A^*$ , the asphericity of the surface-Voronoi cell increases weakly with  $A/A_v$ . For  $A > A^*$ ,  $A_t$  increases as  $A_t=A/A_v$  indicated by the diagonal white line.

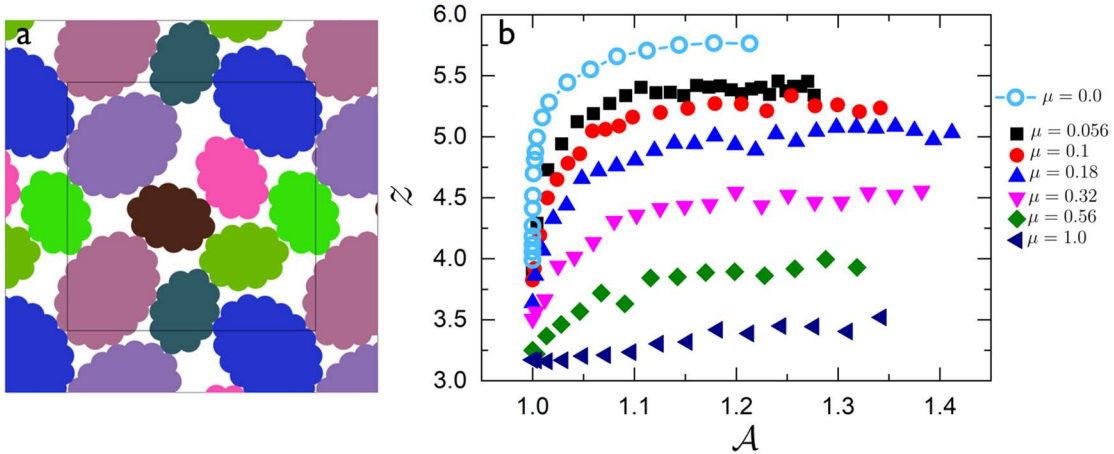


Figure S4: Sample static packing of bidisperse, bumpy ellipses using the rough surface model with size ratio  $r=1.4$ , asphericity  $A=1.08$ , and effective friction coefficient  $\mu=0.4$ . (b) Interparticle contact number  $z$  versus asphericity  $A$  for static packings of smooth and bumpy ellipses with  $N=64$ . The effective friction coefficient  $\mu$  indicates the maximum ratio of the tangential to the normal force over all contacts between bumps on contacting ellipses.

**Shear and bulk moduli:** To calculate the shear modulus  $G$ , we apply a small affine simple shear strain,  $\gamma=10^{-8}$ , with Lees-Edward boundary conditions. After the strain step, we perform energy minimization (to kinetic energy per particle,  $K/N\varepsilon_r < 10^{-20}$ ). The shear modulus is calculated as  $G = 2(U(\gamma)-U(0))/(NA_0\gamma^2)$  where  $A_0$  is the area of the simulation box. To calculate the bulk modulus, we apply a small compressive strain  $\gamma=\Delta L_x/L_x=\Delta L_y/L_y=10^{-8}$ , followed by energy minimization. The bulk modulus is calculated as  $B = 2(U(\gamma)-U(0))/(NA_0\gamma^2)$ . For our studies in 2D, to increase the system size at fixed packing fraction  $\phi$ , we increase the number  $N$  of deformable polygons at fixed edge length of the simulation box  $L$ , and thus the overall size of the deformable polygons decreases as  $p_0 \sim 1/\sqrt{N}$ . To non-dimensionalize the shear ( $G$ ) and bulk ( $B$ ) moduli, we divide them by  $\varepsilon_r/p_0$ , which removes the trivial system size dependence. As noted in the main text, with this non-dimensionalization,  $B$  is roughly independent of system size; however,  $G$  scales as  $N^{-1}$ . System-size scaling of the shear modulus is related to the fact that contacts begin forming and breaking at successively smaller pressures as the system size increases. Similar behavior has also been found for jammed disks in Refs. [33] and [34] in the main text.

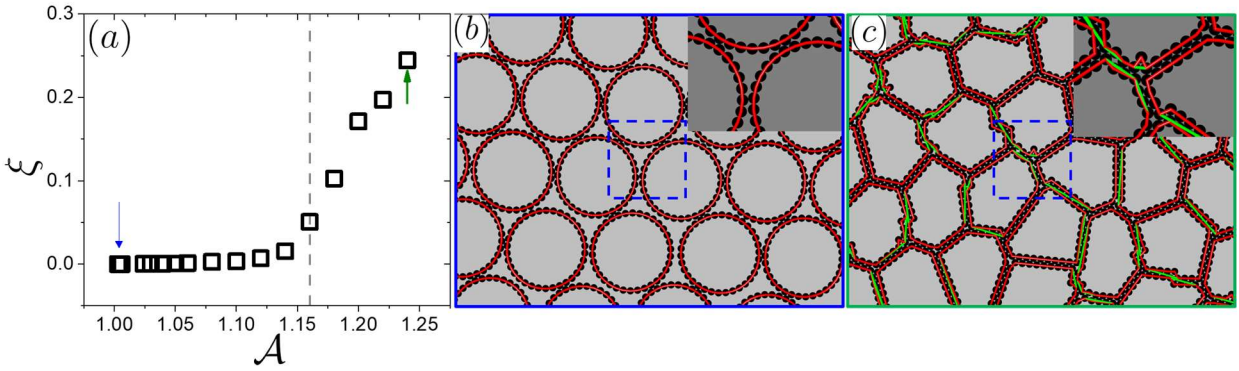
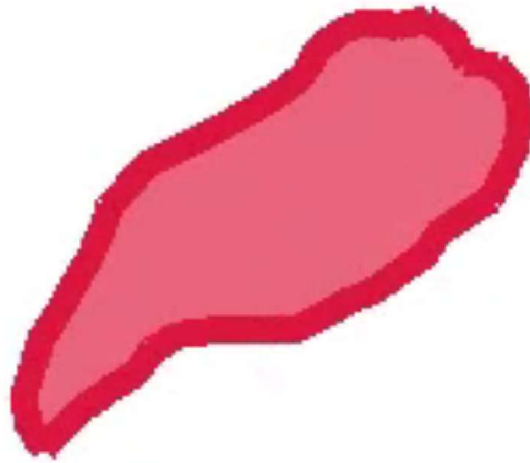


Figure S.5: Excess perimeter  $\xi = p - p_{conv}$  of DP packings (RS model with  $N_v = 34$ ), where  $p_{conv}$  is the perimeter of the DP convex hull, plotted versus  $A$ . The vertical dashed line indicates  $A = 1.16$  and blue and green arrows indicate values of  $A$  for packings in (b) and (c), respectively. The red and green solid lines represent perimeters of the DP and convex hull, respectively. The insets in (b) and (c) are close-ups of the regions indicated by blue-dashed boxes.

The following two movies (Movie S1 and Movie S2) illustrate the capabilities of the DP model for computational studies of single cells, as well as the collective behavior of cell clusters and monolayers.

**Movie S1:** This movie shows the motion of a single deformable particle on a substrate. The particle has  $N_v = 48$  vertices with asphericity,  $A = 5.0$ . Forces are applied to the region of the cell closest to the largest gradient in the nutrient concentration, which fluctuates in time and allows the deformable particle to move on a substrate. The movie file name is Single\_DP.mp4.



**Movie S2:** This movie shows a collection of deformable particles with asphericity  $A = 1.15$  growing uniformly as a cell colony. The movie file name is Collection\_DP.mp4.

